Measurement of the top quark mass using the matrix element technique in dilepton final states

V. M. Abazov,[31] B. Abbott,[67] B. S. Acharya,[25] M. Adams,[46] T. Adams,[44] J. P. Agnew,[41] G. D. Alexeev,[31] G. Alkhazov,[35] A. Alton,[56,a] A. Askew,[44] S. Atkins,[54] K. Augsten,[7] V. Aushev,[38] Y. Aushev,[38] C. Avila,[5] F. Badaud,[10] L. Bagby,[45] B. Baldin,[45] D. V. Bandurin,[74] S. Banerjee,[25] E. Barberis,[55] P. Baringer,[53] J. F. Bartlett,[45] U. Bassler,[15] V. Bazterra,[46] A. Bean,[53] M. Begalli,[2] L. Bellantoni,[45] S. B. Beri,[23] G. Bernardi,[14] R. Bernhard,[19] I. Bertram,[39] M. Besançon,[15] R. Beuselinck,[40] P. C. Bhat,[45] S. Bhatia,[58] V. Bhatnagar,[23] G. Blazey,[47] S. Blessing,[44] K. Bloom,[59] A. Boehnlein,[45] D. Boline,[64] E. E. Boos,[33] G. Borissov,[39] M. Borysova,[38,l] A. Brandt,[71] O. Brandt,[20] M. Brochmann,[75] R. Brock,[57] A. Bross,[45] D. Brown,[14] X. B. Bu,[45] M. Buehler,[45] V. Buescher,[21] V. Bunichev,[33] S. Burdin,[39,b] C. P. Buszello,[37] E. Camacho-Pérez,[28] B. C. K. Casey,[45] H. Castilla-Valdez,[28] S. Caughron,[57] S. Chakrabarti,[64] K. M. Chan,[51] A. Chandra,[73] E. Chapon,[15] G. Chen,[53] S. W. Cho,[27] S. Choi,[27] B. Choudhary,[24] S. Cihangir,[45,*] D. Claes,[59] J. Clutter,[53] M. Cooke,[45,k] W. E. Cooper,[45] M. Corcoran,[73] F. Couderc,[15] M.-C. Cousinou,[12] J. Cuth,[21] D. Cutts,[70] A. Das,[72] G. Davies,[40] S. J. de Jong,[29,30] E. De La Cruz-Burelo,[28] F. Déliot,[15] R. Demina,[63] D. Denisov,[45] S. P. Denisov,[34] S. Desai,[45] C. Deterre,[41,c] K. DeVaughan,[59] H. T. Diehl,[45] M. Diesburg,[45] P. F. Ding,[41] A. Dominguez,[59] A. Dubey,[24] L. V. Dudko,[33] A. Duperrin,[12] S. Dutt,[23] M. Eads,[47] D. Edmunds,[57] J. Ellison,[43] V. D. Elvira,[45] Y. Enari,[14] H. Evans,[49] A. Evdokimov,[46] V. N. Evdokimov,[34] A. Fauré,[15] L. Feng,[47] T. Ferbel,[63] F. Fiedler,[21] F. Filthaut,[29,30] W. Fisher,[57] H. E. Fisk,[45] M. Fortner,[47] H. Fox,[39] J. Franc,[7] S. Fuess,[45] P. H. Garbincius,[45] A. Garcia-Bellido,[63] J. A. García-González,[28] V. Gavrilov,[32] W. Geng,[12,57] C. E. Gerber,[46] Y. Gershtein,[60] G. Ginther,[45] O. Gogota,[38] G. Golovanov,[31] P. D. Grannis,[64] S. Greder,[16] H. Greenlee,[45] G. Grenier,[17] Ph. Gris,[10] J.-F. Grivaz,[13] A. Grohsjean,[15,c] S. Grünendahl,[45] M. W. Grünewald,[26] T. Guillemin,[13] G. Gutierrez,[45] P. Gutierrez,[67] J. Haley,[68] L. Han,[4] K. Harder,[41] A. Harel,[63] J. M. Hauptman,[52] J. Hays,[40] T. Head,[41] T. Hebbeker,[18] D. Hedin,[47] H. Hegab,[68] A. P. Heinson,[43] U. Heintz,[70] C. Hensel,[1] I. Heredia-De La Cruz,[28,d] K. Herner,[45] G. Hesketh,[41,f] M. D. Hildreth,[51] R. Hirosky,[74] T. Hoang,[44] J. D. Hobbs,[64] B. Hoeneisen,[9] J. Hogan,[73] M. Hohlfeld,[21] J. L. Holzbauer,[58] I. Howley,[71] Z. Hubacek,[7,15] V. Hynek,[7] I. Iashvili,[62] Y. Ilchenko,[72] R. Illingworth,[45] A. S. Ito,[45] S. Jabeen,[45,m] M. Jaffré,[13] A. Jayasinghe,[67] M. S. Jeong,[27] R. Jesik,[40] P. Jiang,[*4] K. Johns,[42] E. Johnson,[57] M. Johnson,[45] A. Jonckheere,[45] P. Jonsson,[40] J. Joshi,[43] A. W. Jung,[45,o] A. Juste,[36] E. Kajfasz,[12] D. Karmanov,[33] I. Katsanos,[59] M. Kaur,[23] R. Kehoe,[72] S. Kermiche,[12] N. Khalatyan,[45] A. Khanov,[68] A. Kharchilava,[62] Y. N. Kharzheev,[31] I. Kiselevich,[32] J. M. Kohli,[23] A. V. Kozelov,[34] J. Kraus,[58] A. Kumar,[62] A. Kupco,[8] T. Kurča,[17] V. A. Kuzmin,[33] S. Lammers,[49] P. Lebrun,[17] H. S. Lee,[27] S. W. Lee,[52] W. M. Lee,[45] X. Lei,[42] J. Lellouch,[14] D. Li,[14] H. Li,[74] L. Li,[43] Q. Z. Li,[45] J. K. Lim,[27] D. Lincoln,[45] J. Linnemann,[57] V. V. Lipaev,[*34] R. Lipton,[45] H. Liu,[72] Y. Liu,[4] A. Lobodenko,[35] M. Lokajicek,[8] R. Lopes de Sa,[45] R. Luna-Garcia,[28,g] A. L. Lyon,[45] A. K. A. Maciel,[1] R. Madar,[19] R. Magaña-Villalba,[28] S. Malik,[59] V. L. Malyshev,[31] J. Mansour,[20] J. Martínez-Ortega,[28] R. McCarthy,[64] C. L. McGivern,[41] M. M. Meijer,[29,30] A. Melnitchouk,[45] D. Menezes,[47] P. G. Mercadante,[3] M. Merkin,[33] A. Meyer,[18] J. Meyer,[20,i] F. Miconi,[16] N. K. Mondal,[25] M. Mulhearn,[74] E. Nagy,[12] M. Narain,[70] R. Nayyar,[42] H. A. Neal,[56] J. P. Negret,[5] P. Neustroev,[35] H. T. Nguyen,[74] T. Nunnemann,[22] J. Orduna,[70] N. Osman,[12] A. Pal,[71] N. Parashar,[50] V. Parihar,[70] S. K. Park,[27] R. Partridge,[70,e] N. Parua,[49] A. Patwa,[65,j] B. Penning,[40] M. Perfilov,[33] Y. Peters,[41] K. Petridis,[41] G. Petrillo,[63] P. Pétroff,[13] M.-A. Pleier,[65] V. M. Podstavkov,[45] A. V. Popov,[34] M. Prewitt,[73] D. Price,[41] N. Prokopenko,[34] J. Qian,[56] A. Quadt,[20] B. Quinn,[58] P. N. Ratoff,[39] I. Razumov,[34] I. Ripp-Baudot,[16] F. Rizatdinova,[68] M. Rominsky,[45] A. Ross,[39] C. Royon,[8] P. Rubinov,[45] R. Ruchti,[51] G. Sajot,[11] A. Sánchez-Hernández,[28] M. P. Sanders,[22] A. S. Santos,[1,h] G. Savage,[45] M. Savitskyi,[38] L. Sawyer,[54] T. Scanlon,[40] R. D. Schamberger,[64] Y. Scheglov,[35] H. Schellman,[69,48] M. Schott,[21] C. Schwanenberger,[41] R. Schwienhorst,[57] J. Sekaric,[53] H. Severini,[67] E. Shabalina,[20] V. Shary,[15] S. Shaw,[41] A. A. Shchukin,[34] V. Simak,[7] P. Skubic,[67] P. Slattery,[63] G. R. Snow,[59] J. Snow,[66] S. Snyder,[65] S. Söldner-Rembold,[41] L. Sonnenschein,[18] K. Soustruznik,[6] J. Stark,[11] N. Stefaniuk,[38] D. A. Stoyanova,[34] M. Strauss,[67] L. Suter,[41] P. Svoisky,[74] M. Titov,[15] V. V. Tokmenin,[31] Y.-T. Tsai,[63] D. Tsybychev,[64] B. Tuchming,[15] C. Tully,[61] L. Uvarov,[35] S. Uvarov,[35] S. Uzunyan,[47] R. Van Kooten,[49] W. M. van Leeuwen,[29] N. Varelas,[46] E. W. Varnes,[42] I. A. Vasilyev,[34] A. Y. Verkheev,[31] L. S. Vertogradov,[31] M. Verzocchi,[45] M. Vesterinen,[41] D. Vilanova,[15] P. Vokac,[7] H. D. Wahl,[44] M. H. L. S. Wang,[45] J. Warchol,[51] G. Watts,[75] M. Wayne,[51] J. Weichert,[21] L. Welty-Rieger,[48] M. R. J. Williams,[49,n] G. W. Wilson,[53] M. Wobisch,[54] D. R. Wood,[55] T. R. Wyatt,[41] Y. Xie,[45] R. Yamada,[45] S. Yang,[4] T. Yasuda,[45] Y. A. Yatsunenko,[31] W. Ye,[64] Z. Ye,[45] H. Yin,[45] K. Yip,[65] S. W. Youn,[45] J. M. Yu,[56] J. Zennamo,[62] T. G. Zhao,[41] B. Zhou,[56] J. Zhu,[56] M. Zielinski,[63] D. Zieminska,[49] and L. Zivkovic[14]

(D0 Collaboration)

[1]*LAFEX, Centro Brasileiro de Pesquisas Físicas, Rio de Janeiro, Rio de Janeiro 22290, Brazil*
[2]*Universidade do Estado do Rio de Janeiro, Rio de Janeiro, Rio de Janeiro 20550, Brazil*
[3]*Universidade Federal do ABC, Santo André, São Paulo 09210, Brazil*
[4]*University of Science and Technology of China, Hefei 230026, People's Republic of China*

032004-1

[5]*Universidad de los Andes, Bogotá 111711, Colombia*

[6]*Charles University, Faculty of Mathematics and Physics, Center for Particle Physics,
116 36 Prague 1, Czech Republic*

[7]*Czech Technical University in Prague, 116 36 Prague 6, Czech Republic*

[8]*Institute of Physics, Academy of Sciences of the Czech Republic, 182 21 Prague, Czech Republic*

[9]*Universidad San Francisco de Quito, Quito, Ecuador*

[10]*LPC, Université Blaise Pascal, CNRS/IN2P3, Clermont, F-63178 Aubière Cedex, France*

[11]*LPSC, Université Joseph Fourier Grenoble 1, CNRS/IN2P3, Institut National Polytechnique de
Grenoble, F-38026 Grenoble Cedex, France*

[12]*CPPM, Aix-Marseille Université, CNRS/IN2P3, F-13288 Marseille Cedex 09, France*

[13]*LAL, Univ. Paris-Sud, CNRS/IN2P3, Université Paris-Saclay, F-91898 Orsay Cedex, France*

[14]*LPNHE, Universités Paris VI and VII, CNRS/IN2P3, F-75005 Paris, France*

[15]*CEA Saclay, Irfu, SPP, F-91191 Gif-Sur-Yvette Cedex, France*

[16]*IPHC, Université de Strasbourg, CNRS/IN2P3, F-67037 Strasbourg, France*

[17]*IPNL, Université Lyon 1, CNRS/IN2P3, F-69622 Villeurbanne Cedex, France and Université de Lyon,
F-69361 Lyon CEDEX 07, France*

[18]*III. Physikalisches Institut A, RWTH Aachen University, 52056 Aachen, Germany*

[19]*Physikalisches Institut, Universität Freiburg, 79085 Freiburg, Germany*

[20]*II. Physikalisches Institut, Georg-August-Universität Göttingen, 37073 Göttingen, Germany*

[21]*Institut für Physik, Universität Mainz, 55099 Mainz, Germany*

[22]*Ludwig-Maximilians-Universität München, 80539 München, Germany*

[23]*Panjab University, Chandigarh 160014, India*

[24]*Delhi University, Delhi-110 007, India*

[25]*Tata Institute of Fundamental Research, Mumbai-400 005, India*

[26]*University College Dublin, Dublin 4, Ireland*

[27]*Korea Detector Laboratory, Korea University, Seoul 02841, Korea*

[28]*CINVESTAV, Mexico City 07360, Mexico*

[29]*Nikhef, Science Park, 1098 XG Amsterdam, the Netherlands*

[30]*Radboud University Nijmegen, 6525 AJ Nijmegen, the Netherlands*

[31]*Joint Institute for Nuclear Research, Dubna 141980, Russia*

[32]*Institute for Theoretical and Experimental Physics, Moscow 117259, Russia*

[33]*Moscow State University, Moscow 119991, Russia*

[34]*Institute for High Energy Physics, Protvino, Moscow region 142281, Russia*

[35]*Petersburg Nuclear Physics Institute, St. Petersburg 188300, Russia*

[36]*Institució Catalana de Recerca i Estudis Avançats (ICREA) and Institut de Física d'Altes Energies
(IFAE), 08193 Bellaterra (Barcelona), Spain*

[37]*Uppsala University, 751 05 Uppsala, Sweden*

[38]*Taras Shevchenko National University of Kyiv, Kiev 01601, Ukaine*

[39]*Lancaster University, Lancaster LA1 4YB, United Kingdom*

[40]*Imperial College London, London SW7 2AZ, United Kingdom*

[41]*The University of Manchester, Manchester M13 9PL, United Kingdom*

[42]*University of Arizona, Tucson, Arizona 85721, USA*

[43]*University of California Riverside, Riverside, California 92521, USA*

[44]*Florida State University, Tallahassee, Florida 32306, USA*

[45]*Fermi National Accelerator Laboratory, Batavia, Illinois 60510, USA*

[46]*University of Illinois at Chicago, Chicago, Illinois 60607, USA*

[47]*Northern Illinois University, DeKalb, Illinois 60115, USA*

[48]*Northwestern University, Evanston, Illinois 60208, USA*

[49]*Indiana University, Bloomington, Indiana 47405, USA*

[50]*Purdue University Calumet, Hammond, Indiana 46323, USA*

[51]*University of Notre Dame, Notre Dame, Indiana 46556, USA*

[52]*Iowa State University, Ames, Iowa 50011, USA*

[53]*University of Kansas, Lawrence, Kansas 66045, USA*

[54]*Louisiana Tech University, Ruston, Louisiana 71272, USA*

[55]*Northeastern University, Boston, Massachusetts 02115, USA*

[56]*University of Michigan, Ann Arbor, Michigan 48109, USA*

[57]*Michigan State University, East Lansing, Michigan 48824, USA*

[58]*University of Mississippi, University, Mississippi 38677, USA*

[59]*University of Nebraska, Lincoln, Nebraska 68588, USA*

[60]*Rutgers University, Piscataway, New Jersey 08855, USA*

[61]Princeton University, Princeton, New Jersey 08544, USA
[62]State University of New York, Buffalo, New York 14260, USA
[63]University of Rochester, Rochester, New York 14627, USA
[64]State University of New York, Stony Brook, New York 11794, USA
[65]Brookhaven National Laboratory, Upton, New York 11973, USA
[66]Langston University, Langston, Oklahoma 73050, USA
[67]University of Oklahoma, Norman, Oklahoma 73019, USA
[68]Oklahoma State University, Stillwater, Oklahoma 74078, USA
[69]Oregon State University, Corvallis, Oregon 97331, USA
[70]Brown University, Providence, Rhode Island 02912, USA
[71]University of Texas, Arlington, Texas 76019, USA
[72]Southern Methodist University, Dallas, Texas 75275, USA
[73]Rice University, Houston, Texas 77005, USA
[74]University of Virginia, Charlottesville, Virginia 22904, USA
[75]University of Washington, Seattle, Washington 98195, USA

We present a measurement of the top quark mass in $p\bar{p}$ collisions at a center-of-mass energy of 1.96 TeV at the Fermilab Tevatron collider. The data were collected by the D0 experiment corresponding to an integrated luminosity of 9.7 fb^{-1}. The matrix element technique is applied to $t\bar{t}$ events in the final state containing leptons (electrons or muons) with high transverse momenta and at least two jets. The calibration of the jet energy scale determined in the lepton + jets final state of $t\bar{t}$ decays is applied to jet energies. This correction provides a substantial reduction in systematic uncertainties. We obtain a top quark mass of $m_t = 173.93 \pm 1.84$ GeV.

[*]Deceased.
[a]With visitor from Augustana College, Sioux Falls, SD 57197, USA.
[b]With visitor from The University of Liverpool, Liverpool L69 3BX, United Kingdom.
[c]With visitor from Deutshes Elektronen-Synchrotron (DESY), Notkestrasse 85, Germany.
[d]With visitor from CONACyT, M-03940 Mexico City, Mexico.
[e]With visitor from SLAC, Menlo Park, CA 94025, USA.
[f]With visitor from University College London, London WC1E 6BT, Unted Kingdom.
[g]With visitor from Centro de Investigacion en Computacion—IPN, CP 07738 Mexico City, Mexico.
[h]With visitor from Universidade Estadual Paulista, São Paulo, SP 01140, Brazil.
[i]With visitor from Karlsruher Institut für Technologie (KIT)—Steinbuch Centre for Computing (SCC) D-76128 Karlsruhe, Germany.
[j]With visitor from Office of Science, U.S. Department of Energy, Washington, DC 20585, USA.
[k]With visitor from American Association for the Advancement of Science, Washington, DC 20005, USA.
[l]With visitor from Kiev Institute for Nuclear Research (KINR), Kyiv 03680, Ukraine.
[m]With visitor from University of Maryland, College Park, MD 20742, USA.
[n]With visitor from European Organization for Nuclear Research (CERN), CH-1211 Geneva, Switzerland.
[o]With visitor from Purdue University, West Lafayette, IN 47907, USA.

I. INTRODUCTION

The top quark is the heaviest elementary particle of the standard model (SM) [1–5]. Its mass (m_t) is a free parameter of the SM Lagrangian that is not predicted from first principles. The top quark was discovered in 1995 by the CDF and D0 Collaborations at the Tevatron $p\bar{p}$ collider at Fermilab [6,7]. Despite the fact that the top quark decays weakly, its large mass leads to a very short lifetime of approximately 5×10^{-25} s [8–10]. It decays into a W boson and a b quark before hadronizing, a process that has a characteristic time scale of $1/\Lambda_{\text{QCD}} \approx (200 \text{ MeV})^{-1}$, equivalent to $\tau_{\text{had}} \approx 3.3 \times 10^{-24}$ s, where Λ_{QCD} is the fundamental scale of quantum chromodynamics (QCD). This provides an opportunity to measure the mass of the top quark with high precision due to the possibility of reconstructing the top quark parameters using its decay particles.

At the Tevatron, top quarks are produced mainly as $t\bar{t}$ pairs through the strong interaction. At leading order (LO) in perturbative QCD, a pair of top quarks is produced via quark-antiquark ($q\bar{q}$) annihilation with a probability of about 85% [11,12] or via gluon-gluon (gg) fusion.

Final states of $t\bar{t}$ production are classified according to the decays of the two W bosons. This results in final states with two, one, or no leptons, which are referred to as the dilepton ($\ell\ell$), lepton + jets (ℓ + jets), and all-jet channels, respectively. In this measurement, we use events in the dilepton final state where both W bosons decay to leptons: $t\bar{t} \to W^+ b W^- \bar{b} \to \ell^+ \nu_\ell b \ell^- \bar{\nu}_\ell \bar{b}$. More specifically, we

consider three combinations of leptons, *ee*, *eμ*, and *μμ*, including also electrons and muons from leptonic decays of *τ* leptons, $W \to \tau\nu_\tau \to \ell\nu_\ell\nu_\tau$. We present an updated measurement of the top quark mass in the dilepton channel using the matrix element (ME) approach [13]. This measurement improves the previous result using the matrix element technique with 5.3 fb^{-1} of integrated luminosity [14] by a factor of 1.6, where the statistical uncertainty is improved by a factor of 1.1 and systematic uncertainty by a factor of 2.7. The most precise m_t measurement by the D0 experiment based on this method was performed in ℓ + jets analysis [1,2]. The CMS Collaboration has applied a different approach for measuring m_t in the dilepton channel, obtaining a precision of 1.23 GeV [4].

This measurement uses the entire data set accumulated by the D0 experiment during run II of the Fermilab Tevatron collider, corresponding to an integrated luminosity of 9.7 fb^{-1}. We use the final D0 jet energy scale (JES) corrections and the refined corrections of the *b* quark jet energy scale [15]. The measurement is performed with a blinded approach, as described in Sec. IV. Similarly to the recent top mass measurement in the dilepton final state using a neutrino weighting technique [16], we correct jet energies by a calibration factor obtained in the top quark mass measurement in the ℓ + jets analysis [1,2].

II. DETECTOR AND EVENT SAMPLES

A. D0 detector

The D0 detector is described in detail in Refs. [17–23]. It has a central tracking system consisting of a silicon microstrip tracker and a central fiber tracker, both located within a 2 T superconducting solenoidal magnet. The central tracking system is designed to optimize tracking and vertexing at detector pseudorapidities of $|\eta_{\text{det}}| < 2.5$.[1] A liquid-argon sampling calorimeter has a central section (CC) covering $|\eta_{\text{det}}|$ up to ≈1.1, and two end calorimeters (EC) that extend coverage to $|\eta_{\text{det}}| \approx 4.2$, with all three housed in separate cryostats. An outer muon system, with pseudorapidity coverage of $|\eta_{\text{det}}| < 2$, consists of a layer of tracking detectors and scintillation trigger counters in front of 1.8 T iron toroids, followed by two similar layers after the toroids.

The sample of $p\bar{p}$ collision data considered in this analysis is split into four data-taking periods: run IIa, run IIb1, run IIb2, and run IIb3 with the corresponding integrated luminosities given in Table I. All event simulations are split according to these epochs to better model changes of detector response with time, such as the addition of an additional SMT layer [20] or the reconstruction

---

[1]The pseudorapidity is defined as $\eta = -\ln[\tan(\theta/2)]$, where θ is the polar angle of the reconstructed particle originating from a primary vertex relative to the proton beam direction. Detector pseudorapidity η_{det} is defined relative to the center of the detector instead of the primary vertex.

TABLE I. The integrated luminosity and the jet energy scale correction factor k_{JES}, averaged over e + jets and μ + jets channels [1,2], for the four separate data-taking periods.

Data-taking period	Integrated luminosity, pb^{-1}	k_{JES}
runIIa	1081	0.993 ± 0.016
runIIb1	1223	1.027 ± 0.013
runIIb2	3034	1.033 ± 0.008
runIIb3	4398	1.026 ± 0.006

algorithm performance variations due to increasing luminosity [24].

B. Object identification

Top pair events in the dilepton channel contain two isolated charged leptons, two *b* quark jets, and a significant imbalance in transverse momentum ($\not{p}_T$) due to escaping neutrinos.

Electrons are identified as energy clusters in the calorimeter within a cone of radius $\mathcal{R} = \sqrt{(\Delta\eta)^2 + (\Delta\phi)^2} = 0.2$ (where ϕ is the azimuthal angle) that are consistent in their longitudinal and transverse profiles with expectations from electromagnetic showers. More than 90% of the energy of an electron candidate must be deposited in the electromagnetic part of the calorimeter. The electron is required to be isolated by demanding that less than 20% of its energy is deposited in an annulus of $0.2 < \mathcal{R} < 0.4$ around its direction. This cluster has to be matched to a track reconstructed in the central tracking system. We consider electrons in the CC with $|\eta_{\text{det}}| < 1.1$ and in the EC with $1.5 < |\eta_{\text{det}}| < 2.5$. The transverse momenta of electrons (p_T^e) must be greater than 15 GeV. In addition, we use a multivariate discriminant based on tracking and calorimeter information to reject jets misidentified as electrons. It has an electron selection efficiency between 75% and 80%, depending on the data-taking period, rapidity of the electron, and number of jets in the event. The rejection rate for jets is approximately 96%.

Muons are identified [24] as segments in at least one layer of the muon system that are matched to tracks reconstructed in the central tracking system. Reconstructed muons must have $p_T > 15$ GeV, $|\eta| < 2$, and satisfy the two following isolation criteria. First, the transverse energy deposited in the calorimeter annulus $0.1 < \mathcal{R} < 0.4$ around the muon ($E_T^{\mu,\text{iso}}$) must be less than 15% of the transverse momentum of the muon (p_T^μ). Secondly, the sum of the transverse momenta of the tracks in a cone of radius $\mathcal{R} = 0.5$ around the muon track in the central tracking system ($p_T^{\mu,\text{iso}}$) must be less than 15% of p_T^μ.

Jets are identified as energy clusters in the electromagnetic and hadronic parts of the calorimeter, reconstructed using an iterative mid-point cone algorithm with radius $\mathcal{R} = 0.5$ [25]. An external JES correction is determined by calibrating the energy deposited in the jet cone using

transverse momentum balance in exclusive photon + jet and dijet events in data [15]. When a muon track overlaps the jet cone, twice the p_T of the muon is added to the jet p_T, assuming that the muon originates from a semileptonic decay of a hadron belonging to the jet and that the neutrino has the same p_T as the muon. In addition, we use the difference in single-particle responses between data and Monte Carlo (MC) simulation to provide a parton-flavor-dependent JES correction [15]. This correction significantly reduces the bias in the jet energy and the total JES uncertainty of the jets initiated by b quarks. Jet energies in simulated events are also corrected for residual differences in energy resolution and energy scale between data and simulation. These correction factors are measured by comparing data and simulation in Drell-Yan ($Z/\gamma^\star \to ee$) events with accompanying jets [15].

The typical JES uncertainty is approximately 2%. We improve this by calibrating the jet energy after event selection through a constant scale factor k_{JES} measured in the lepton + jets final state using jets associated with W boson decay [1,2]. This approach was first applied in Ref. [26]. We apply the k_{JES} factor to the jet p_T in data as $p_T^{\mathrm{corr}} = p_T/k_{\mathrm{JES}}$, independently for each data-taking period. We use the correction factors averaged over e + jets and μ + jets final states (Table I). The uncertainties related to the determination and propagation of the k_{JES} scale factor are accounted for as systematic uncertainties and described in Sec. V.

We use a multivariate analysis (MVA) technique to identify jets originating from b quarks [27,28]. The algorithm combines the information from the impact parameters of tracks and from variables that characterize the properties of secondary vertices within jets. Jet candidates for b tagging are required to have at least two tracks with $p_T > 0.5$ GeV originating from the vertex of the $p\bar{p}$ interaction, and to be matched to a jet reconstructed from just the charged tracks.

The missing transverse momentum, $\not{p}_T$, is reconstructed from the energy deposited in the calorimeter cells, and all corrections to p_T for leptons and jets are propagated into a revised $\not{p}_T$. A significance in $\not{p}_T$, symbolized by $\sigma_{\not{p}_T}$, is defined through a likelihood ratio based on the $\not{p}_T$ probability distribution, calculated from the expected resolution in $\not{p}_T$ and the energies of electrons, muons, and jets.

C. Event selection

We follow the approach developed in Ref. [29] to select dilepton events, using the criteria listed below:

(i) For the ee and $\mu\mu$ channels, we select events that pass at least one single-lepton trigger, while for the $e\mu$ channel we consider events selected through a mixture of single and multilepton triggers and lepton + jet triggers. Efficiencies for single electron and muon triggers are measured using $Z/\gamma^\star \to ee$ or $Z/\gamma^\star \to \mu\mu$ data and found to be $\approx 99\%$ and $\approx 80\%$,

respectively, in dilepton events. For the $e\mu$ channel, the trigger efficiency is $\approx 100\%$.

(ii) We require at least one $p\bar{p}$ interaction vertex in the interaction region with $|z| < 60$ cm, where z is the coordinate along the beam axis, and $z = 0$ is the center of the detector. At least three tracks with $p_T > 0.5$ GeV must be associated with this vertex.

(iii) We require at least two isolated leptons with $p_T > 15$ GeV, both originating from the same interaction vertex. The two highest-p_T leptons must have opposite electric charges.

(iv) To reduce the background from bremsstrahlung in the $e\mu$ final state, we require the distance in (η, ϕ) space between the electron and the muon trajectories to be $\mathcal{R}(e, \mu) > 0.3$.

(v) We require the presence of at least two jets with $p_T > 20$ GeV and $|\eta_{\mathrm{det}}| < 2.5$.

(vi) The $t\bar{t}$ final state contains two b quark jets. To improve the separation between signal and background, we apply a selection using the b quark jet identification MVA discriminant to demand that at least one of the two jets with highest p_T is b tagged [27,28]. The b tagging helps significantly in rejecting Z boson related backgrounds. We apply requirements on the MVA variable that provide b quark jet identification efficiencies of 84% in $e\mu$, 80% in ee, and 78% in $\mu\mu$ final states, with background misidentifications rates of 23%, 12%, and 7%, respectively.

(vii) Additional selection criteria based on global event properties further improve the signal purity. In $e\mu$ events, we require $H_T > 110$ GeV, where H_T is the scalar sum of the p_T of the leading lepton and the two leading jets. In the ee final state, we require $\sigma_{\not{p}_T} > 5$, while in the $\mu\mu$ channel, we require $\not{p}_T > 40$ GeV and $\sigma_{\not{p}_T} > 2.5$.

(viii) In rare cases, the numerical integration of the matrix elements described in Sec. III A may yield extremely small probabilities that prevent us from using the event in the analysis. We reject such events using a selection that has an efficiency of 99.97% for simulated $t\bar{t}$ signal samples. For background MC events, the efficiency is 99.3%. No event is removed from the final data sample because of this requirement.

D. Simulation of signal and background events

The main sources of background in the $\ell\ell$ channel are Drell-Yan production ($q\bar{q} \to (Z/\gamma^\star \to \ell\ell)$ + jets), diboson production (WW, WZ, and ZZ), and instrumental background. The instrumental background arises mainly from ($W \to \ell\nu$) + jets and multijet events, in which one or two jets are misidentified as electrons, or where muons or electrons originating from semileptonic decays of heavy-flavor hadrons appear to be isolated. To estimate the $t\bar{t}$ signal efficiency and the background contamination, we use MC simulation for all contributions, except for

the instrumental background, which is estimated from data.

The number of expected $t\bar{t}$ signal events is estimated using the LO matrix element generator ALPGEN (version v2.11) [30] for the hard-scattering process, with up to two additional partons, interfaced with the PYTHIA generator [31] (version 6.409, with a D0 modified Tune A [32]) for parton showering and hadronization. The CTEQ6M parton distribution functions (PDF) [33,34] are used in the event generation, with the top quark mass set to 172.5 GeV. The next-to-next-to LO (NNLO) $t\bar{t}$ cross section of $7.23^{+0.11}_{-0.20}$ pb [35] is used for the normalization. For the calibration of the ME method, we also use events generated at $m_t = 165$, 170, 175, and 180 GeV. Those samples are simulated in the same way as the sample with the $m_t = 172.5$ GeV. Drell-Yan samples are also simulated using ALPGEN (version 2.11) for the hard-scattering process, with up to three additional partons, and the PYTHIA (version 6.409, D0 modified Tune A) generator for parton showering and hadronization. We separately generate processes corresponding to Z-boson production with heavy flavor partons, $(Z \to \ell\ell) + b\bar{b}$ and $(Z \to \ell\ell) + c\bar{c}$, and light flavor partons. Samples with light partons only are generated separately for the parton multiplicities of 0, 1, 2 and 3, samples with the heavy flavor partons are generated including additional 0, 1 and 2 light partons. The MC cross sections for all Drell-Yan samples are scaled up with a next-to-LO (NLO) K factor of 1.3, and cross sections for heavy-flavor samples are scaled up with additional K factors of 1.52 for $(Z \to \ell\ell) + b\bar{b}$ and 1.67 for $(Z \to \ell\ell) + c\bar{c}$, as estimated with the MCFM program [36]. In the simulation of diboson events, the PYTHIA generator is used for both hard scattering and parton showering. To simulate effects from additional overlapping $p\bar{p}$ interactions, "zero bias" events are selected randomly in collider data and overlaid on the simulated events. Generated MC events are processed using a GEANT3-based [37] simulation of the D0 detector.

E. Estimation of instrumental background contributions

In the ee and $e\mu$ channels, we determine the contributions from events in data with jets misidentified as electrons through the "matrix method" [38]. A sample of events (n_{loose}) is defined using the same selections as given for $t\bar{t}$

candidates in items (i)–(vii) above, but omitting the requirement on the electron MVA discriminant. For the dielectron channel, we drop the MVA requirement on one of the randomly-chosen electrons.

Using $Z/\gamma^\star \to ee$ data, we measure the efficiency ε_e that events with electrons must pass the requirements on the electron MVA discriminant. We measure the efficiency f_e that events with no electron pass the electron MVA requirement by using $e\mu$ events selected with criteria (i)–(v), but requiring leptons of same electric charge. We also apply a reversed isolation requirement to the muon, $E_T^{\mu,\text{iso}}/p_T^\mu > 0.2$, $p_T^{\mu,\text{iso}}/p_T^\mu > 0.2$, and $\not{p}_T < 15$ GeV, to minimize the contribution from $W +$ jets events.

We extract the number of events with misidentified electrons (n_f), and the number of events with true electrons (n_e), by solving the equations

$$n_{\text{loose}} = n_e/\varepsilon_e + n_f/f_e,$$
$$n_{\text{tight}} = n_e + n_f, \tag{1}$$

where n_{tight} is the number of events remaining after implementing selections (i)–(vii). The factors f_e and ε_e are measured for each jet multiplicity (0, 1, and 2 jets), and separately for electron candidates in the central and end sections of the calorimeter. Typical values of ε_e are 0.7–0.8 in the CC and 0.65–0.75 in the EC. Values of f_e are 0.005–0.010 in the CC, and 0.005–0.020 in the EC.

In the $e\mu$ and $\mu\mu$ channels, we determine the number of events with an isolated muon arising from decays of hadrons in jets by relying on the same selection as for the $e\mu$ or $\mu\mu$ channels, but requiring that both leptons have the same charge. In the $\mu\mu$ channel, the number of background events is taken to be the number of same-sign events. In the $e\mu$ channel, it is the number of events in the same-sign sample after subtracting the contribution from events with misidentified electrons in the same way as it is done in Ref. [39].

To use the ME technique, we need a pool of events to calculate probabilities corresponding to the instrumental background. In the $e\mu$ channel, we use the loose sample defined above to model misidentified electron background. Using this selection we obtain a background sample of 2901 events. In the $\mu\mu$ channel, the estimated number of multijet and $W +$ jets background events is zero (Table II). In the ee channel, the number of such events is too small to provide a representative instrumental background sample.

TABLE II. The numbers of expected background and $t\bar{t}$ events, and the number of events observed in data. The NNLO cross section is used to normalize the $t\bar{t}$ content. Systematic uncertainties are shown for all the expected numbers.

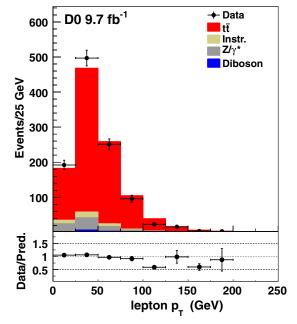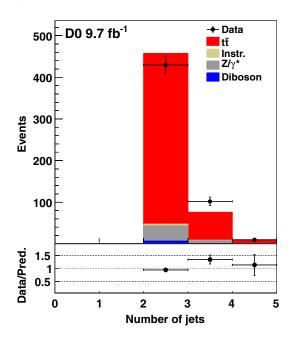|	$Z/\gamma^\star +$ jets	Diboson	Instr.	$t\bar{t}$	Total	Data
$e\mu$	$13.0^{+1.7}_{-1.6}$	$3.7^{+0.8}_{-0.8}$	$16.4^{+4.0}_{-4.0}$	$260.6^{+22.5}_{-16.3}$	$293.8^{+23.5}_{-17.7}$	346
ee	$13.8^{+2.1}_{-1.9}$	$1.9^{+0.4}_{-0.2}$	$1.8^{+0.2}_{-0.2}$	$88.0^{+9.1}_{-8.2}$	$105.5^{+10.3}_{-9.5}$	104
$\mu\mu$	$10.6^{+1.3}_{-1.4}$	$1.7^{+0.4}_{-0.4}$	$0^{+0.05}_{-0.05}$	$76.0^{+6.2}_{-4.1}$	$88.3^{+6.7}_{-4.7}$	92
$\ell\ell$	$37.4^{+5.1}_{-4.9}$	$7.3^{+1.6}_{-1.6}$	$18.2^{+4.0}_{-4.0}$	$424.6^{+37.8}_{-28.6}$	$487.6^{+40.5}_{-31.9}$	545

FIG. 1.   The distributions in lepton p_T and the ratio of data to predictions for the combined ee, $e\mu$, and $\mu\mu$ final states after applying requirements (i)–(vii).
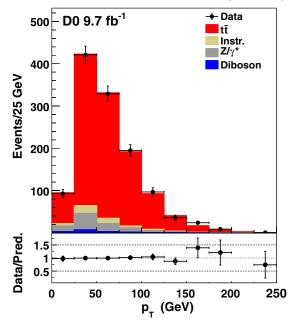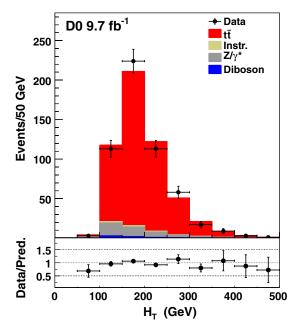

FIG. 3.   The distributions in jet p_T after implementing the k_{JES} correction, and the ratio of data to the prediction for the combined ee, $e\mu$, and $\mu\mu$ final states after applying requirements (i)–(vii).

Instead we increase the number of background events due to Z-boson production by the corresponding amount in the calibration procedure.

F. Sample composition

The numbers of predicted background events as well as the expected numbers of signal events for the final selection

in $e\mu$, $\mu\mu$, and ee channels are given in Table II. They show the high signal purity of the selected sample. The $e\mu$ channel has a relatively low fraction of the $Z/\gamma^\star$ + jets background events because the electron and muon are produced through the cascade decay of the τ-lepton, $Z/\gamma^\star \rightarrow \tau\tau \rightarrow e\mu\nu_e\nu_\mu$. Comparisons between distributions measured in data and predictions after the final selection are shown in Figs. 1–4 for the combined ee, $e\mu$, and $\mu\mu$

FIG. 2.   The distributions in the number of jets and the ratio of data to the prediction for the combined ee, $e\mu$, and $\mu\mu$ final states after applying requirements (i)–(vii).

FIG. 4.   The distributions in H_T after implementing the k_{JES} correction, and the ratio of data to the prediction for the combined ee, $e\mu$, and $\mu\mu$ final states after applying requirements (i)–(vii).

channels. Only statistical uncertainties are shown. The predicted number of $t\bar{t}$ and background events is normalized to the number of events found in data. The jet p_T and H_T distributions in Figs. 3 and 4 are shown after applying the k_{JES} correction from the ℓ + jets analysis [1,2].

III. MASS DETERMINATION METHOD

A. Matrix element technique

This measurement uses the matrix element technique [13]. This method provides the most precise m_t measurement at the Tevatron in the ℓ + jets final state [1,2], and was applied in previous measurement of m_t in the dilepton final state using 5.3 fb^{-1} of integrated luminosity [14]. The ME method used in this analysis is described below.

B. Event probability calculation

The ME technique assigns a probability to each event, which is calculated as

$$P(x, f_{t\bar{t}}, m_t) = f_{t\bar{t}} \cdot P_{t\bar{t}}(x, m_t) + (1 - f_{t\bar{t}}) \cdot P_{\text{bkg}}(x), \quad (2)$$

where $f_{t\bar{t}}$ is the fraction of $t\bar{t}$ events in the data, and $P_{t\bar{t}}$ and P_{bkg} are the respective per-event probabilities calculated under the hypothesis that the selected event is either a $t\bar{t}$ event, characterized by a top quark mass m_t, or background. Here, x represents the set of measured observables, i.e., p_T, η, and ϕ for jets and leptons. We assume that the masses of top quarks and antitop quarks are the same. The probability $P_{t\bar{t}}(x, m_t)$ is calculated as

$$P_{t\bar{t}}(x, m_t) = \frac{1}{\sigma_{\text{obs}}(m_t)} \int f_{\text{PDF}}(q_1) f_{\text{PDF}}(q_2)$$
$$\times \frac{(2\pi)^4 |\mathcal{M}(y, m_t)|^2}{q_1 q_2 s} W(x, y) d\Phi_6 dq_1 dq_2, \quad (3)$$

where q_1 and q_2 represent the respective fractions of proton and antiproton momenta carried by the initial state partons, f_{PDF} represents the parton distribution functions, and y refers to partonic four-momenta of the final-state objects. The detector transfer functions (TF), $W(x, y)$, correspond to the probability for reconstructing parton four-momenta y as the final-state observables x. The term $d\Phi_6$ represents the six-body phase space, and $\sigma_{\text{obs}}(m_t)$ is the $t\bar{t}$ cross section observed at the reconstruction level, calculated using the matrix element $\mathcal{M}(y, m_t)$, corrected for selection efficiency. The LO matrix element $\mathcal{M}(y, m_t)$ for the processes $q\bar{q} \to t\bar{t} \to W^+ W^- b\bar{b} \to \ell^+ \ell^- \nu_\ell \bar{\nu}_\ell b\bar{b}$ is used in our calculation [40] and it contains a Breit-Wigner function to represent each W boson and top quark mass. The matrix element is averaged over the colors and spins of the initial state partons, and summed over the colors and spins of the final state partons. The gg matrix element is neglected, since it comprises only 15% of the total $t\bar{t}$ production cross

section at the Tevatron. Including it does not significantly improve the statistical sensitivity of the method.

The electron momenta and the directions of all reconstructed objects are assumed to be perfectly measured and are therefore represented through δ functions, $\delta(x - y)$, reducing thereby the dimensionality of the integration. This leaves the magnitues of the jet and muon momenta to be modelled. Following the same approach as in the previous measurement [14], we parametrize the jet energy resolution by a sum of two Gaussian functions with parameters depending linearly on parton energies, while the resolution in the curvature of the muon $(1/p_T^\mu)$ is described by a single Gaussian function. All TF parameters are determined from simulated $t\bar{t}$ events. We use the same parametrizations for the transfer functions as in the ℓ + jets m_t measurement. The detailed description of the TFs is given in Ref. [2].

The masses of the six final state particles are set to 0 except for the b quark jets, for which a mass of 4.7 GeV is used. We integrate over eight dimensions in the ee channel, nine in the $e\mu$ channel, and ten in the $\mu\mu$ channel. As integration variables we use the top and antitop quark masses, the W^+ and W^- boson masses, the transverse momenta of the two jets, the p_T and ϕ of the $t\bar{t}$ system, and $1/p_T^\mu$ for muons. This choice of variables differs from that of the previous measurement [14], providing a factor of ≈ 100 reduction in integration time.

To reconstruct the masses of the top quarks and W bosons, we solve the kinematic equations analytically by summing over the two possible jet-parton assignments and over all real solutions for each neutrino momentum [41]. If more than two jets exist in the event, we use only the two with highest transverse momenta. The integration is performed using the MC based numerical integration algorithm VEGAS [42,43], as implemented in the GNU Scientific Library [44].

Since the dominant source of background in the dilepton final state is from $Z/\gamma^\star$ + jets events, as can be seen from Table II, we consider only the $Z/\gamma^\star$ + jets matrix element in the calculation of the background probability, $P_{\text{bkg}}(x)$. The LO $(Z/\gamma^\star \to \ell\ell) + 2$ jets ME from the VECBOS generator [45] is used in this analysis. In the $e\mu$ channel, background events are produced through the $(Z/\gamma^\star \to \tau\tau \to \ell\ell) + 2$ jets processes. Since $Z/\gamma^\star \to \tau\tau$ decays are not implemented in VECBOS, we use an additional transfer function to describe the energy of the final state lepton relative to the initial τ lepton, obtained from parton-level information [41]. As for $P_{t\bar{t}}(x, m_t)$, the directions of the jets and charged leptons are assumed to be well-measured, and each kinematic solution is weighted according to the p_T of the $Z/\gamma^\star$ + jets system. The integration of the probability $P_{\text{bkg}}(x)$ is performed over the energies of the two partons initiating the selected jets and both possible assignments of jets to top quark decays.

The normalization of the background per-event probability could be defined in the same way as for the signal probabilities, i.e. by dividing the probabilities by σ_{obs}.

However, the calculation of the integral equivalent to Eq. (3) for the background requires significant computational resources, and therefore a different approach is chosen. We use a large ensemble including $t\bar{t}$ and background events in known proportion. We fit the fraction of background events in the ensemble by adjusting the background normalization. The value which minimizes the difference between the fitted signal fraction and the true one is chosen as the background normalization factor (see Ref. [46] for more details).

C. Likelihood evaluation and m_t extraction

To extract the top quark mass from a set of n events with measured observables $x_1, ..., x_n$, we construct a log-likelihood function from the event probabilities:

$$-\ln L(x_1,...,x_n; f_{t\bar{t}}, m_t) = -\sum_{i=1}^{n} \ln(P_{\text{evt}}(x_i; f_{t\bar{t}}, m_t)). \quad (4)$$

This function is minimized with respect to the two free parameters $f_{t\bar{t}}$ and m_t. To calculate the signal probabilities, we use step sizes of 2.5 GeV for m_t and 0.004 for $f_{t\bar{t}}$. The minimum value of the log-likelihood function, m_{lhood}, is fitted using a second degree polynomial function, in which $f_{t\bar{t}}$ is fixed at its fitted value. The statistical uncertainty on the top quark mass, σ_{lhood}, is given by the difference in the mass at $-\ln L_{\min}$ and at $-\ln L_{\min} + 0.5$. The m_t extractions are done separately for ee, $e\mu$, and $\mu\mu$ final states and for the combination of all three channels.

D. Method calibration

We calibrate the method to correct for biases in the measured mass and statistical uncertainty through an ensemble testing technique. We generate datalike ensembles with simulated signal and background events, measure the top quark mass m_{lhood}^i and its uncertainty σ_{lhood}^i in each ensemble i through the minimization of the log-likelihood function, and calculate the following quantities:

(i) The mean value m_{mean} of the m_{lhood}^i distribution. Comparing m_{mean} with the input in the simulation determines the bias in m_t.

(ii) The mean value Δm_t of the uncertainty distribution in σ_{lhood}^i. This quantity characterizes the expected uncertainty in the measured top quark mass.

(iii) The standard deviation of the distribution of the pull variable, w_{pull}, or pull width, where the pull variable is defined as $w_{\text{pull}} = (m_{\text{lhood}}^i - m_{\text{mean}})/\sigma_{\text{lhood}}^i$, provides a correction to the statistical uncertainty σ_{lhood}.

We use resampling (multiple uses of a given event) when generating the ensembles. In the D0 MC simulation, a statistical weight w_j is associated with each event j, which is given by the product of the MC cross section weight, simulation-to-data efficiency corrections and other simulation-to-data correction factors. The probability for an event to be used in the ensemble is proportional to its

weight w_j. Multiple use of the events significantly reduces the uncertainty of the ensemble testing procedure for a fixed number of ensembles, but leads to the overestimation of the statistical precision, for which we account through a dedicated correction factor.
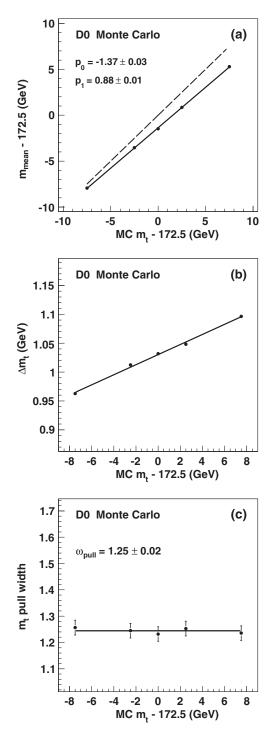

FIG. 5. The response of the ME method in (a) m_t, (b) statistical uncertainty on the m_t, and (c) the pull width, shown as a function of the MC input m_t for the combined ee, $e\mu$, and $\mu\mu$ channels. The error bars in (a) and (b) are invisibly small. The dashed line in (a) represents the case of ideal response.

TABLE III. The expected statistical uncertainties for a generated $m_t = 172.5$ GeV for the ee, $e\mu$, and $\mu\mu$ channels and their combination.

Final state	ee	$e\mu$	$\mu\mu$	$\ell\ell$
Uncertainty, GeV	3.69	1.71	3.57	1.45

We use 1000 ensembles per MC input mass m_t, with the number of events per ensemble equal to the number of events selected in data. In each ensemble, the number of events from each background source is generated following multinomial statistics, using the expected number of background events in Table II. The number of $t\bar{t}$ events is calculated as the difference between the total number of events in the ensemble and the generated number of background events. We combine all three channels to construct a joint calibration curve. Using MC samples generated at five MC m_t, we determine a linear calibration between the measured and generated masses: $m_{\mathrm{mean}} - 172.5$ GeV $= p_0 + p_1(\mathrm{MC}m_t - 172.5)$ GeV. The relations obtained for the combination of the $e\mu$, ee, and $\mu\mu$ final states are shown in Fig. 5. The difference of the calibration curve from the ideal case demonstrates that the method suffers from some biases.

The expected statistical uncertainty for the generated top quark mass of 172.5 GeV is calculated as $\Delta m_t^{\mathrm{exp}} = \Delta m_t(172.5 \text{ GeV}) \cdot w_{\mathrm{pull}}/p_1$, and given in Table III.

IV. FIT TO DATA

The fit to data is first performed using an unknown random offset in the measured mass. This offset is removed only after the final validation of the methodology. We apply the ME technique to data as follows:

TABLE IV. The calibrated top quark mass for the ee, $e\mu$, and $\mu\mu$ channels, and for their combination. The quoted uncertainties are statistical.

Final state	Mass (GeV)
ee	176.94 ± 4.65
$e\mu$	172.18 ± 1.95
$\mu\mu$	176.04 ± 4.82
$\ell\ell$	173.93 ± 1.61

(i) The k_{JES} correction factor from the lepton + jets mass analysis [1,2] is applied to the jet p_T in data as $p_T^{\mathrm{corr}} = p_T/k_{\mathrm{JES}}$ (Sec. II). The uncertainties related to the propagation of this correction from ℓ + jets to the dilepton final state are included in the systematic uncertainties as a residual JES uncertainty and statistical uncertainty on k_{JES} scale factor discussed in Sec. V B.

(ii) The calibration correction from Fig. 5 is applied to m_{lhood} and σ_{lhood} to obtain the measured values:

$$m_{\mathrm{meas}} = (m_{\mathrm{lhood}} - p_0 - 172.5)/p_1 + 172.5(\mathrm{GeV}),$$
$$\sigma_{\mathrm{meas}} = \sigma_{\mathrm{lhood}} \cdot w_{\mathrm{pull}}/p_1. \tag{5}$$

(iii) The fit to the log-likelihood function is the best fit to a parabola in an interval containing a 10 GeV range in MC m_t around the minimum before its calibration.

The log-likelihood function in data is shown in Fig. 6. Table IV shows the results for each channel separately and for their combination. The distribution in the expected statistical uncertainty for an input MC top quark mass of 175 GeV (the closest input value to the mass obtained in data) for the three combined channels is shown in Fig. 7.

FIG. 6. The negative log-likelihood ratio for the combined ee, $e\mu$, and $\mu\mu$ data after calibration, as a function of the input MC m_t. The curve is the best fit to a parabola in the interval 168.4–179.7 GeV.

FIG. 7. The distribution in the expected statistical uncertainty $\sigma_{\mathrm{lhood}}^{\mathrm{exp}}$ for the combined ee, $e\mu$, and $\mu\mu$ channels after applying calibration, for the MC input $m_t = 175$ GeV. The arrow indicates the statistical uncertainty for data after the calibration (σ_{meas}).

V. SYSTEMATIC UNCERTAINTIES AND RESULTS

Systematic uncertainties affect the measured m_t in two ways. First, the distribution in the signal and background log-likelihood functions can be affected directly by a change in some parameter, leading to a bias in the calibration. Second, the signal-to-background ratio in the selected data can be affected by the parameter change, leading to a difference in the combined signal and background log-likelihood function, again causing a a bias in the calibration. Ideally, these two contributions can be treated coherently for each source of systematic uncertainty, but since the second effect is much smaller than the first for the most important systematic uncertainties, we keep the same signal-to-background ratio in pseudo-experiments, except for the systematic uncertainty in the signal fraction. Background events are included in the evaluation of all sources of systematic uncertainty, and all systematic uncertainties are evaluated using the simulated events with a top quark mass of 172.5 GeV.

A. Systematic uncertainties in modeling signal and background

We determine uncertainties related to signal modeling by comparing simulations with different generators and parameters, as described below.

(i) Higher-order corrections. By default, we use LO ALPGEN to model signal events. To evaluate the effect of higher-order corrections on the top quark mass, we use signal events generated with the NLO MC generator MC@NLO (version 3.4) [47,48], interfaced to HERWIG (version 6.510) [49] for parton showering and hadronization. The CTEQ6M PDFs [33,34] are used to generate events at a top quark mass of $m_t = 172.5$ GeV. Because MC@NLO is interfaced to HERWIG for simulating the showering contributions to the process of interest, we use ALPGEN+HERWIG events for this comparison, in order to avoid double-counting an uncertainty due to a different showering model.

(ii) Initial state radiation (ISR) and final-state radiation (FSR). This systematic uncertainty is evaluated comparing the result using ALPGEN+PYTHIA by changing the factorization and renormalization scale parameters, up and down by a factor of 2, as done in Ref. [2].

(iii) Hadronization and underlying event. The systematic uncertainty due to the hadronization and the underlying event (UE) is estimated as the difference between m_t measured using the default ALPGEN+PYTHIA events and events generated using different hadronization models. We consider three alternatives: ALPGEN+HERWIG, ALPGEN+PYTHIA using Perugia Tune 2011C (with color reconnection), or

using Perugia Tune 2011NOCR (without color reconnection) [50]. We take the largest of these differences, which is the difference relative to ALPGEN+ HERWIG, as an estimate of the systematic uncertainty for choice of effects from the hadronization and the UE.

(iv) Color reconnection. We estimate the effect of the model for color reconnection (CR) by comparing the top quark mass measured with ALPGEN+ PYTHIA Perugia Tune 2011C (with color reconnection), and with Perugia Tune 2011NOCR (without color reconnection) [50]. Our default ALPGEN+ PYTHIA tune does not have explicit CR modeling, so we consider Perugia2011NOCR as the default in this comparison.

(v) Uncertainty in modeling b quark fragmentation (b quark jet modeling). Uncertainties in simulation of b quark fragmentation can affect the m_t measurement through b quark jet identification or transfer functions. This is studied using the procedure described in Ref. [51] by reweighting b quark fragmentation to match a Bowler scheme tuned to either LEP or SLD data.

(vi) PDF uncertainties. The systematic uncertainty due to the choice of PDF is estimated by changing the 20 eigenvalues of the CTEQ6.1M PDF within their uncertainties in $t\bar{t}$ MC simulations. Ensemble tests are repeated for each of these changes and the total uncertainty is evaluated as in Ref. [2].

(vii) Transverse momentum of the $t\bar{t}$ system. To evaluate this systematic uncertainty, we reconstruct the $t\bar{t}$ p_T from the two leading jets, two leading leptons, and $\not{p}_T$. The distribution in the MC events is reweighted to match that in data using a linear fit to the p_T distribution of the $t\bar{t}$ system. To improve statistics, we combine all the dilepton channels for the extraction of the reweighting function.

(viii) Heavy-flavor scale factor. In the ALPGEN ($Z/\gamma^\star \to \ell\ell$) + jets background samples, the fraction of heavy-flavor events is not well modelled. Therefore, a heavy-flavor scale factor is applied to the ($Z \to \ell\ell$) + $b\bar{b}$ and ($Z/\gamma^\star \to \ell\ell$) + $c\bar{c}$ cross sections to increase the heavy-flavor content. This scale factor has an uncertainty of $\pm 20\%$. We estimate its systematic effect by changing the scale factor within this uncertainty.

(ix) Multiple $p\bar{p}$ interactions. Several independent $p\bar{p}$ interactions in the same bunch crossing may influence the measurement of m_t. We reweight the number of interactions in simulated MC samples to the number of interactions found in data before implementing any selection requirements. To estimate the effect from a possible mismatch in luminosity profiles, we examine the distribution in instantaneous luminosity in both data and MC after

event selection, and reweight the instantaneous luminosity profile in MC events to match data.

B. JES systematic uncertainties

The relative difference between the JES in data and MC simulations is described by the k_{JES} factor extracted in the $\ell+$ jets mass measurement [1,2]. As mentioned above, we apply this scale factor to jet p_T in data. In the previous dilepton analysis [14], the JES and the ratio of b and light jet responses were the dominant systematic uncertainties. The improvements made in the jet calibration [15] and use of the k_{JES} factor in the dilepton channel reduce the uncertainty related to the JES from 1.5 to 0.5 GeV.

(i) Residual uncertainty in JES. This uncertainty arises from the fact that the JES depends on the p_T and η of the jet. The JES correction in the $\ell+$ jets measurement assumes a constant scale factor, i.e., we correct the average JES, but not the p_T and η dependence. In addition, the k_{JES} correction can be affected by the different jet p_T requirements on jets in the $\ell+$ jets and in dilepton final states. There can also be a different JES offset correction due to different jet multiplicities. We estimate these uncertainties as follows. We use MC events in which the jet energies are shifted upward by one standard deviation of the $\gamma+$ jet JES uncertainty and correct jet p_T in these samples to $p_T^{\mathrm{corr\ MC}}=p_T^{\mathrm{MC}}\cdot k_{\mathrm{JES}}^{\mathrm{UP}}/k_{\mathrm{JES}}$, where $k_{\mathrm{JES}}^{\mathrm{UP}}$ is the JES correction measured in the $\ell+$ jets analysis for the MC events that are shifted up by one standard deviation. The $1/k_{\mathrm{JES}}$ factor appears because the k_{JES} is applied to the data and not to MC samples. Following the same approach as in [15], we assume that the downward change for the JES samples has the same effect as the upward changes in jet p_T.

(ii) Uncertainty on the $\boldsymbol{k_{\mathrm{JES}}}$ factor. The statistical uncertainty on the k_{JES} scale factor is 0.5%–1.5% depending on the data-taking period (Table I). We recalculate the mass measured in MC with the k_{JES} correction shifted by one standard deviation. This procedure is applied separately for each data-taking period, and the uncertainties are summed in quadrature.

(iii) Ratio of $\boldsymbol{b}$ and light jet responses or flavor-dependent uncertainty. The JES calibration used in this measurement contains a flavor-dependent jet response correction, which accounts for the difference in detector response to different jet flavors, in particular b quark jets versus light-quark jets. This correction is applied to the jets in MC simulation through a convolution of the corrections for all simulated particles associated to the jet as a function of particle p_T and η. It is constructed in a way that preserves the flavor-averaged JES corrections for $\gamma+$ jets events [15]. The k_{JES} correction does not improve this calibration, because it is

measured in light jet flavor from $WW\rightarrow qq'$ decays. To propagate the effect of the uncertainty to the measured m_t value, we change the corresponding correction by the size of the uncertainty and recalculate m_t.

C. Object reconstruction and identification

(i) Trigger. To evaluate the impact of the trigger on our analysis, we scale the number of background events according to the uncertainty on the trigger efficiency for different channels. The number of signal $t\bar{t}$ events is recalculated as the difference between the number of events in data and the expected number of background events. We reconstruct ensembles according to the varied event fractions and extract the new mass.

(ii) Electron momentum scale and resolution. This uncertainty reflects the difference in the absolute lepton momentum measurement and the simulated resolution [52] between data and MC events. We estimate this uncertainty by changing the corresponding parameters up and down by one standard deviation for the simulated samples, and assigning the difference in the measured mass as a systematic uncertainty.

(iii) Systematic uncertainty in $\boldsymbol{p_T}$ resolution of muons. We estimate the uncertainty by changing the muon p_T resolution [24] by ±1 standard deviation in the simulated samples and assign the difference in the measured mass as a systematic uncertainty.

(iv) Jet identification. Scale factors are used to correct the jet identification efficiency in MC events. We estimate the systematic uncertainty by changing these scale factors by ±1 standard deviation.

(v) Systematic uncertainty in jet resolution. The procedure of correction of jet energies for residual differences in energy resolution and energy scale in simulated events [15] applies additional smearing to the MC jets in order to account for the differences in jet p_T resolution in data and MC. To compute the systematic uncertainty on the jet resolution, the parameters for jet energy smearing are changed by their uncertainties.

(vi) b-tagging efficiency. A difference in b-tagging modeling between data and simulation may case a systematic change in m_t. To estimate this uncertainty, we change the b tagging corrections up and down within their uncertainties using reweighting.

D. Method

(i) MC calibration. An estimate of the statistical uncertainties from the limited size of MC samples used in the calibration procedure is obtained through the statistical uncertainty of the calibration parameters. To determine this contribution, we propagate the

uncertainties on the calibration constants p_0 and p_1 (Fig. 5) to m_t.

(ii) Instrumental background. To evaluate systematic uncertainty due to instrumental background, we change its contribution by $\pm25\%$. The number of signal $t\bar{t}$ events is recalculated by subtracting the instrumental background from the number of events in data, and ensemble studies are repeated to extract m_t.

(iii) Background contribution (or signal fraction). To propagate the uncertainty associated with the background level, we change the number of background events according to its uncertainty, rerun the ensembles, and extract m_t. In the ensembles, the number of $t\bar{t}$ events is defined by the difference in the observed number of events in data and the expected number of background events.

E. MC statistical uncertainty estimation

We evaluated MC statistical uncertainties in the estimation of systematic uncertainties. To obtain the MC statistical uncertainty in the $t\bar{t}$ samples, we divide each sample into independent subsets. The dispersion of masses in these subsets is used to estimate the uncertainty. The estimated MC statistical uncertainties for the signal modeling and jet and electron energy resolution are 0.11–0.14 GeV, for all other the typical uncertainty is around 0.04 GeV. In cases when the obtained estimate of MC statistical uncertainty is larger than the value of the systematic uncertainty, we take the MC statistical uncertainty as the systematic uncertainty.

F. Summary of systematic uncertainties

Table V summarizes all contributions to the uncertainty on the m_t measurement with the ME method. Each source is corrected for the slope of the calibration from Fig. 5(a). The uncertainties are symmetrized in the same way as in the $\ell +$ jets measurement [1,2]. We use sign $\pm$ if the positive variation of the source of uncertainty corresponds to a positive variation of the measured mass, and $\mp$ if it corresponds to a negative variation for two-sided uncertainties. We quote the uncertainties for one sided sources or the ones dominated by one-side component in Table V, indicating the direction of m_t change when using an alternative instead of the default model. As all the entries in the total systematic uncertainty are independent, the total systematic uncertainty on the top mass measurement is obtained by adding all the contributions in quadrature.

VI. CONCLUSION

We have performed a measurement of the top quark mass in the dilepton channel $t\bar{t} \to W^+bW^-\bar{b} \to \ell^+\nu_\ell b\ell^-\bar{\nu}_\ell \bar{b}$ using the matrix element technique in 9.7 fb^{-1} of integrated luminosity collected by the D0 detector at the Fermilab Tevatron $p\bar{p}$ Collider. The result $m_t = 173.93 \pm 1.61(\text{stat}) \pm 0.88(\text{syst})$ GeV, corresponding to a relative precision of 1.0%, is consistent with the values of the current Tevatron [5] and world combinations [3].

TABLE V. Systematic and statistical uncertainties for the measurement of m_t in dilepton final states. The values are given for the combination of the ee, $e\mu$, and $\mu\mu$ channels.

Source	Uncertainty (GeV)
Signal and background modeling:	
Higher order corrections	$+0.16$
ISR/FSR	±0.16
Hadronization and UE	$+0.31$
Color Reconnection	$+0.15$
b-jet modelling	$+0.21$
PDF uncertainty	±0.20
Heavy flavor	∓0.06
$p_T(t\bar{t})$	$+0.03$
Multiple $p\bar{p}$ interactions	-0.10
Detector modeling:	
Residual jet energy scale	-0.20
Uncertainty on k_{JES} factor	∓0.46
Flavor-dependent jet response	∓0.30
Jet energy resolution	∓0.15
Electron momentum scale	∓0.10
Electron resolution	∓0.16
Muon resolution	∓0.10
b-tagging efficiency	∓0.28
Trigger	±0.06
Jet ID	$+0.08$
Method:	
MC calibration	±0.03
Instrumental background	±0.07
MC background	±0.06
Total systematic uncertainty	±0.88
Total statistical uncertainty	±1.61
Total uncertainty	±1.84

[1] V. M. Abazov *et al.* (D0 Collaboration), Precision Measurement of the Top-Quark Mass in lepton + jets Final States, Phys. Rev. Lett. **113**, 032002 (2014).

[2] V. M. Abazov *et al.* (D0 Collaboration), Precision measurement of the top-quark mass in lepton + jets final states, Phys. Rev. D **91**, 112003 (2015).

[3] ATLAS Collaboration, CDF Collaboration, CMS Collaboration, and D0 Collaboration, First combination of Tevatron and LHC measurements of the top-quark mass, arXiv:1403.4427.

[4] V. Khachatryan *et al.* (CMS Collaboration), Measurement of the top quark mass using proton-proton data at $\sqrt{(s)} = 7$ and 8 TeV, Phys. Rev. D **93**, 072004 (2016).

[5] CDF and D0 collaborations, Combination of CDF and D0 results on the mass of the top quark using up to 9.7 fb^{-1} at the Tevatron, arXiv:1407.2682.

[6] S. Abachi *et al.* (D0 Collaboration), Observation of the Top Quark, Phys. Rev. Lett. **74**, 2632 (1995).

[7] F. Abe *et al.* (CDF Collaboration), Observation of Top Quark Production in $\bar{p}p$ Collisions, Phys. Rev. Lett. **74**, 2626 (1995).

[8] M. Jezabek and J. H. Kühn, Semileptonic decays of top quarks, Phys. Lett. B **207**, 91 (1988).

[9] M. Jezabek and J. H. Kühn, QCD corrections to semileptonic decays of heavy quarks, Nucl. Phys. **314**, 1 (1989).

[10] V. M. Abazov *et al.* (D0 Collaboration), An improved determination of the width of the top quark, Phys. Rev. D **85**, 091104 (2012).

[11] W. Bernreuther, A. Brandenburg, Z. G. Si, and P. Uwer, Top quark pair production and decay at hadron colliders, Nucl. Phys. **690**, 81 (2004).

[12] M. Czakon, M. L. Mangano, A. Mitov, and J. Rojo, Constraints on the gluon PDF from top quark pair production at hadron colliders, J. High Energy Phys. 07 (2013) 167.

[13] V. M. Abazov *et al.* (D0 Collaboration), A precision measurement of the mass of the top quark, Nature (London) **429**, 638 (2004).

[14] V. M. Abazov *et al.* (D0 Collaboration), Precise Measurement of the Top Quark Mass in the Dilepton Channel at D0, Phys. Rev. Lett. **107**, 082004 (2011).

[15] V. M. Abazov *et al.* (D0 Collaboration), Jet energy scale determination in the D0 experiment, Nucl. Instrum. Methods Phys. Res., Sect. A **763**, 442 (2014).

[16] V. M. Abazov *et al.* (D0 Collaboration), Precise measurement of the top quark mass in dilepton decays using optimized neutrino weighting, Phys. Lett. B **752**, 18 (2016).

[17] V. M. Abazov *et al.* (D0 Collaboration), The upgraded D0 detector, Nucl. Instrum. Methods Phys. Res., Sect. A **565**, 463 (2006).

[18] V. M. Abazov *et al.*, The muon system of the run II D0 detector, Nucl. Instrum. Methods Phys. Res., Sect. A **552**, 372 (2005).

[19] M. Abolins *et al.*, Design and implementation of the new D0 level-1 calorimeter trigger, Nucl. Instrum. Methods Phys. Res., Sect. A **584**, 75 (2008).

[20] R. Angstadt *et al.*, The layer 0 inner silicon detector of the D0 experiment, Nucl. Instrum. Methods Phys. Res., Sect. A **622**, 298 (2010).

[21] S. Ahmed *et al.* (D0 Collaboration), The D0 silicon microstrip tracker, Nucl. Instrum. Methods Phys. Res., Sect. A **634**, 8 (2011).

[22] B. Casey *et al.*, The D0 run IIb luminosity measurement, Nucl. Instrum. Methods Phys. Res., Sect. A **698**, 208 (2013).

[23] V. Bezzubov, D. Denisov, V. Evdokimov, V. Lipaev, A. Shchukin, and I. Vasilyev, The performance and long term stability of the D0 run II forward muon scintillation counters, Nucl. Instrum. Methods Phys. Res., Sect. A **753**, 105 (2014).

[24] V. M. Abazov *et al.* (D0 Collaboration), Muon reconstruction and identification with the Run II D0 detector, Nucl. Instrum. Methods Phys. Res., Sect. A **737**, 281 (2014).

[25] G. C. Blazey *et al.*, Run II Jet Physics, in *Proceedings of the Workshop on QCD and Weak Boson Physics in Run II*, edited by U. Baur *et al.* (2000), p. 47, arXiv:hep-ex/0005012.

[26] V. M. Abazov *et al.* (D0 Collaboration), Measurement of the top quark mass in $p\bar{p}$ collisions using events with two leptons, Phys. Rev. D **86**, 051103 (2012).

[27] V. M. Abazov *et al.* (D0 Collaboration), *b*-Jet Identification in the D0 Experiment, Nucl. Instrum. Methods Phys. Res., Sect. A **620**, 490 (2010).

[28] V. M. Abazov *et al.* (D0 Collaboration), Improved *b* quark jet identification at the D0 experiment, Nucl. Instrum. Methods Phys. Res., Sect. A **763**, 290 (2014).

[29] V. M. Abazov *et al.* (D0 Collaboration), Measurement of the $t\bar{t}$ production cross section using dilepton events in $p\bar{p}$ collisions, Phys. Lett. B **704**, 403 (2011).

[30] M. L. Mangano, M. Moretti, F. Piccinini, R. Pittau, and A. D. Polosa, ALPGEN, a generator for hard multiparton processes in hadronic collisions, J. High Energy Phys. 07 (2003) 001.

[31] T. Sjöstrand, S. Mrenna, and P. Z. Skands, PYTHIA 6.4 physics and manual, J. High Energy Phys. 05 (2006) 026.

[32] T. Affolder *et al.* (CDF Collaboration), Charged jet evolution and the underlying event in $p\bar{p}$ collisions at 1.8 TeV, Phys. Rev. D **65**, 092002 (2002).

[33] J. Pumplin, D. R. Stump, J. Huston, H.-L. Lai, P. Nadolsky, and W.-K. Tung, New generation of parton distributions with uncertainties from global QCD analysis, J. High Energy Phys. 07 (2002) 012.

[34] P. M. Nadolsky, H.-L. Lai, Q.-H. Cao, J. Huston, J. Pumplin, D. Stump, W.-K. Tung, and C.-P. Yuan, Implications of CTEQ global analysis for collider observables, Phys. Rev. D **78**, 013004 (2008).

[35] M. Czakon and A. Mitov, Top++: A program for the calculation of the top-pair cross-section at hadron colliders, Comput. Phys. Commun. **185**, 2930 (2014).

[36] R. K. Ellis, An update on the next-to-leading order Monte Carlo MCFM, Nucl. Phys. B, Proc. Suppl. **160**, 170 (2006).

[37] R. Brun and F. Carminati, CERN Report No. W5013, 1993.

[38] V. M. Abazov *et al.* (D0 Collaboration), Measurement of the $t\bar{t}$ production cross section in $p\bar{p}$ collisions at $\sqrt{s} =$ 1.96-TeV using kinematic characteristics of lepton + jets events, Phys. Rev. D **76**, 092007 (2007).

[39] V. M. Abazov *et al.* (D0 Collaboration), Measurement of the asymmetry in angular distributions of leptons produced in dilepton $t\bar{t}$ final states in $p\bar{p}$ collisions at $\sqrt{s} = 1.96$ TeV, Phys. Rev. D **88**, 112002 (2013).

[40] G. Mahlon and S. J. Parke, Maximizing spin correlations in top quark pair production at the Tevatron, Phys. Lett. B **411**, 173 (1997).

[41] F. Fiedler, A. Grohsjean, P. Haefner, and P. Schieferdecker, The Matrix Element Method and its Application in Measurements of the Top Quark Mass, Nucl. Instrum. Methods Phys. Res., Sect. A **624**, 203 (2010).

[42] G. Lepage, A new algorithm for adaptive multidimensional integration, J. Comput. Phys. **27**, 192 (1978).

[43] G. Lepage, VEGAS: An adaptive multi-dimensional integration program (1980), Cornell preprint CLNS 80-447.

[44] M. Galassi, J. Davies, J. Theiler, B. Gough, G. Jungman, P. Alken, M. Booth, and F. Rossi, *GNU Scientific Library Reference Manual*, 3rd ed. (Network Theory Ltd., 2009).

[45] F. A. Berends, H. Kuijf, B. Tausk, and W. T. Giele, On the production of a W and jets at hadron colliders, Nucl. Phys. **B357**, 32 (1991).

[46] A. Grohsjean, Measurement of the top quark mass in the dilepton final state using the matrix element method, Fermilab thesis, 2008.

[47] S. Frixione and B. R. Webber, Matching NLO QCD computations and parton shower simulations, J. High Energy Phys. 06 (2002) 029.

[48] S. Frixione and B. R. Webber, The MC@NLO 3.4 event generator, arXiv:0812.0770.

[49] G. Corcella, I. G Knowles, G. Marchesini, S. Moretti, K. Odagiri, P. Richardson, M. H Seymour, and B. R Webber, HERWIG 6.5: An event generator for hadron emission reactions with interfering gluons (including supersymmetric processes), J. High Energy Phys. 01 (2001) 010.

[50] P. Z. Skands, Tuning Monte Carlo generators: The Perugia tunes, Phys. Rev. D **82**, 074018 (2010).

[51] Y. Peters, K. Hamacher, and D. Wicke, Report No. FERMI-LAB-TM-2425-E, 2006.

[52] V. M. Abazov *et al.* (D0 Collaboration), Electron and photon identification in the D0 experiment, Nucl. Instrum. Methods Phys. Res., Sect. A **750**, 78 (2014).